



Physicochemical studies of molecular hyperpolarizability of imidazole derivatives

Jayaraman Jayabharathi*, Venugopal Thanikachalam, Natesan Srinivasan, Marimuthu Venkatesh Perumal, Karunamoorthy Jayamoorthy

Department of Chemistry, Annamalai University, Annamalainagar, 608 002 Tamilnadu, India

ARTICLE INFO

Article history:

Received 22 November 2010

Received in revised form 12 February 2011

Accepted 15 February 2011

Keywords:

NMR

DFT

NLO

NBO

Occupation coefficients

Vibrational analysis

ABSTRACT

A series of substituted imidazoles have been synthesized in very good yield under solvent free condition by grinding 1,2-diketone, arylaldehyde, arylamine and ammonium acetate in the presence of molecular iodine as the catalyst. The short reaction time, good yield and easy workup make this protocol practically and economically attractive and the imidazoles are characterized by NMR spectra, X-ray, mass and CHN analysis. The push–pull character of series of imidazoles have been analyzed by the quotient of the occupations of the bonding (π) and anti-bonding (π^*) orbitals of the central linking $-N=C-C=C-$ unit. Excellent correlation of the push–pull parameter with the corresponding bond lengths $d_{C=N}$ and $d_{C=C}$ strongly recommend both the occupation quotients (π^*/π) and the corresponding bond lengths are reasonable sensors for quantifying the push–pull character and for the molecular hyperpolarizability β_0 of these compounds. To support the experimental results, theoretical calculations (heat of formation, NLO, NBO and vibrational analysis) were also made. Within this context, reasonable conclusions concerning the steric hindrance in the chromospheres, push–pull character, hyperpolarizability of the imidazoles and their application as NLO materials will be drawn.

© 2011 Elsevier B.V. All rights reserved.

1. Introduction

Designing of “green” experimental protocol is an enormous challenge to chemists to improve the quality of the environment for present and future generations. Compounds with an imidazole ring system have many pharmacological properties [1,2]. Though there are several methods reported [3,4] in the literature for the synthesis of imidazoles, they suffer from one or more disadvantages such as harsh reaction conditions, poor yields, prolonged time period, use of hazardous and often expensive acid catalysts. Since organic solvents are high on the list of damaging chemicals, in recent years solid-state organic reactions have caused great interest. Recently, molecular iodine received considerable attention as an inexpensive, nontoxic, readily available catalyst for various organic transformations, affording the corresponding products in excellent yields with high selectivity. Owing to numerous advantages associated with this eco-friendly element, iodine has been explored as a powerful catalyst for various organic transformations [5]. During the course of our studies towards the development of new route to the synthesis of biologically active heterocycles, we wish to report a simple and an efficient method for the synthesis of substituted imi-

dazoles using iodine as the catalyst. Searching for organic materials with nonlinear optical (NLO) properties is usually concentrated on molecules with donor–acceptor π -conjugation (D– π –A) and deals with the systematic investigation of substituent effects on the degree of π -conjugation, steric hindrance and the hyperpolarizability of the substances. Besides, geometrical arrangement of the molecules in the solid state, their interaction and other physicochemical properties (e.g. strong intramolecular charge-transfer absorptions) and engineering possibilities are also important [6]. At present, there is an insufficient understanding of all influences for designing optimal NLO materials, even if the influencing factors in certain classes of D– π –A compounds were theoretically studied [7]. To quantify the push–pull effect in D– π –A compounds, bond length alternation (BLA) and out-of-plane distortions of the polarized C=C double bonds, available from X-ray studies, have been employed for a long time [8]. Alternatively, dipole moment measurements [9], bond lengths [10], barriers to rotation about the partial C=C double bonds [11] (from dynamic NMR studies), and the occupation quotients (π/π^*) [12] of the bonding (to quantify the acceptor activity) and anti-bonding orbital (to quantify the donor activities) of these C=C double bonds were adopted. Not only the push–pull effect in D– π –A compounds could be quantified, but also a linear dependence of the push–pull quotient (π^*/π) on molar hyperpolarizability of these compounds were detected [13]. Thus, π^*/π proves to be an easily accessible, general and sensitive

* Corresponding author. Tel.: +91 9443940735.

E-mail address: jtchalam2005@yahoo.co.in (J. Jayabharathi).

parameter of the donor–acceptor quality of compounds for potential NLO applications. Furthermore, we have reported the Quantum chemical analysis [14] (DFT/B3LYP) method with 6-311G++ (d,p) as basis set) of imidazole derivatives **1–6** (heat of formation, geometrical structure, vibration wave numbers, NLO and NBO analysis) and the optimized geometrical parameters obtained by DFT calculation is in good agreement with single crystal XRD data. The Mulliken and NBO charge analysis were also calculated and discussed about the more basic nature of the nitrogen atom of the imidazole derivatives. The electric dipole moment (μ) and the first-hyperpolarizability (β) value of the investigated molecules have been studied by both experimentally and theoretically which reveal that they have non-linear optical (NLO) behavior with non-zero values. These chromophores possess a more appropriate ratio of off – diagonal versus diagonal β tensorial component ($r = \beta_{xyy}/\beta_{xxx}$) which reflects the inplane nonlinearity anisotropy since they have largest $\mu\beta_0$ values, the reported imidazoles can be used as potential NLO materials.

2. Experimental

2.1. Optical measurements and composition analysis

NMR spectra were recorded for the imidazole derivatives (**1–6**) on a Bruker 400 MHz. The ultraviolet-visible (UV–Vis) spectra were measured on a UV–Vis spectrophotometer (Perkin Elmer, Lambda 35) and corrected for background due to solvent absorption. Mass spectra were recorded on a Varian Saturn 2200 GCMS spectrometer.

2.2. Non-linear optical measurements

The second harmonic generation efficiency was assessed by Kurtz powder technique [15] at IISc., Bangalore, India. It is a well established tool to evaluate the conversion efficiency of non-linear optical materials. A Q-switched Nd:YAG laser operating at the fundamental wavelength of 1064 nm, generating about 4.1 mJ and pulse width of 8 ns was used for the present experimental study. The input laser beam was passed through an IR reflector and then incident on the powder form of the specimen, which was packed in a glass capillary tube. The output energy was detected by a photodiode detector integrated with oscilloscope assembly.

2.3. Computational details

Quantum mechanical calculations were carried out using Gaussian-03 program [14]. As the first step of our DFT calculation, the geometry taken from the starting structure was optimized.

2.3.1. Hyperpolarizability calculation

The density functional theory has been used to calculate the dipole moment (μ), mean polarizability (α) and the total first static hyperpolarizability (β) [16] for **1–6** in terms of x, y, z components and are given by following equations.

$$\mu = (\mu_x^2 + \mu_y^2 + \mu_z^2)^{1/2} \quad (1)$$

$$\alpha = \frac{1}{3}(\alpha_{xx} + \alpha_{yy} + \alpha_{zz}) \quad (2)$$

$$\beta_{tot} = (\beta_x^2 + \beta_y^2 + \beta_z^2)^{1/2} \quad (\text{or}) \quad \beta_{tot} = [(\beta_{xxx} + \beta_{xyy} + \beta_{xzz})^2 + (\beta_{yyy} + \beta_{yzz} + \beta_{yxx})^2 + (\beta_{zzz} + \beta_{zxx} + \beta_{zyy})^2]^{1/2} \quad (3)$$

The β components of Gaussian output are reported in atomic units and therefore the calculated values are converted into e.s.u. units ($1 \text{ a.u.} = 8.3693 \times 10^{-33} \text{ e.s.u.}$).

2.3.2. Natural Bond Orbital (NBO) analysis

The second order Fock matrix was carried out to evaluate the donor–acceptor interactions in the NBO analysis [17]. For each donor (i) and acceptor (j), the stabilization energy $E(2)$ associated with the delocalization $i \rightarrow j$ is estimated as

$$E(2) = \Delta E_{ij} = q_i \frac{F(i, j)^2}{\epsilon_j - \epsilon_i} \quad (4)$$

where q_i is the donor orbital occupancy, ϵ_i and ϵ_j are diagonal elements and $F(i, j)$ is the off diagonal NBO Fock matrix element. The larger the $E(2)$ value, the more intensive is the interaction between electron donors and electron acceptors.

2.3.3. General procedure for the synthesis of 2-aryl imidazole derivatives (**1–6**)

A mixture of substituted aldehyde (1 mmol), benzil (1 mmol), ammonium acetate (2.5 mmol) and iodine (15 mol %) were grained in a mortar at room temperature for appropriate time. The reaction was monitored by TLC and the reaction mixture was treated with aqueous $\text{Na}_2\text{S}_2\text{O}_3$, the formed crude was purified by column chromatography (n-hexane:ethyl acetate (9:1) (Scheme 1).

2.3.4. 2-(4-Fluorophenyl)-4,5-dimethyl-1-p-tolyl-1H-imidazole (**1**)

Yield: 50%. mp 130 °C, Anal. calcd. for $\text{C}_{18}\text{H}_{17}\text{FN}_2$: C, 77.12; H, 6.11; N, 9.99. Found: C, 77.00; H, 5.98; N, 9.03. FTIR (cm^{-1}) 1519, 1598, 1647, 2364, 2855, 2916, 3540, 3751. ^1H NMR (400 MHz, CDCl_3): δ 2.01 (s, 3H), 2.29 (s, 3H), 2.43 (s, 3H), 6.87–7.34 (aromatic protons). ^{13}C (100 MHz, CDCl_3): δ 9.53, 12.69, 21.18, 114.92, 115.10, 125.44, 127.16, 129.89, 130.20, 133.35, 135.13, 138.57, 144.28, 161.26, 163.23. MS: m/z 280.00, calcd. 280.14.

2.3.5. 2-(4-Fluorophenyl)-1,4,5-triphenyl-1H-imidazole (**2**)

Yield: 60%. mp 242 °C, Anal. calcd. for $\text{C}_{27}\text{H}_{19}\text{FN}_2$: C, 83.05; H, 4.90; N, 7.17. Found: C, 82.00; H, 5.00; N, 4.78. FTIR (cm^{-1}) 1256, 1645, 2434, 2990, 3456. ^1H NMR (400 MHz, CDCl_3): δ 6.92 (d, 2H), 7.49–7.80 (m, 15H), 7.90 (d, 2H) (aromatic protons). ^{13}C (100 MHz, CDCl_3): δ 126.55, 127.38, 128.10, 128.38, 128.93, 130.69, 131.12, 134.46, 137.14, 138.29, 146.91. MS: m/z 390.00, calcd. 390.45.

2.3.6. 2-(4,5-Diphenyl-1H-imidazol-2-yl)phenol (**3**)

Yield: 62%. mp 210 °C, Anal. calcd. for $\text{C}_{21}\text{H}_{16}\text{N}_2\text{O}$: C, 80.75; H, 5.16; N, 8.97. Found: C, 79.12; H, 5.20; N, 7.64. FTIR (cm^{-1}) 1640, 2462, 3008, 3462, 3658. ^1H NMR (400 MHz, CDCl_3): δ 6.93–6.99 (m, 7H), 7.26–7.52 (m, 7H), 8.04 (s, 1H), 12.97 (brs, 1H) (aromatic protons), ^{13}C (100 MHz, CDCl_3): δ 113.36, 117.29, 119.32, 125.42, 129.09, 130.54, 146.33, 157.17. MS: m/z 312.00, calcd. 312.36.

2.3.7. 2-(4,5-Diphenyl-1-p-tolyl-1H-imidazol-2-yl)phenol (**4**)

Yield: 65%. mp 215 °C, Anal. calcd. for $\text{C}_{28}\text{H}_{22}\text{N}_2\text{O}$: C, 83.56; H, 5.51; N, 6.96. Found: C, 83.00; H, 5.20; N, 6.02. FTIR (cm^{-1}) 1638, 2465, 2996, 3456, 3598. ^1H NMR (400 MHz, CDCl_3): δ 2.27 (s, 3H), 6.80 (d, 2H), 7.84 (d, 2H), 7.16–7.25 (m, 7H), 7.45–7.51 (m, 6H), 9.31 (s, 1H), 12.50 (brs, 1H) (aromatic protons), ^{13}C (100 MHz, CDCl_3): δ 9.53, 114.73, 120.80, 126.06, 126.33, 127.15, 127.40, 145.87, 157.08. MS: m/z 402.00, calcd. 402.17.

2.3.8.

2-(2-Methoxyphenyl)-4,5-diphenyl-1-p-tolyl-1H-imidazole (**5**)

Yield: 62%. mp 235 °C, Anal. calcd. for $\text{C}_{29}\text{H}_{24}\text{N}_2\text{O}$: C, 83.63; H, 5.81; N, 6.73. Found: C, 82.98; H, 5.01; N, 6.01. FTIR (cm^{-1}) 1230, 1450, 1605, 2924, 3512, 3614. ^1H NMR (400 MHz, CDCl_3): δ 2.20 (s, 3H), 3.80 (s, 3H), 2.40 (s, 3H), 6.77 (d, 2H), 7.05–7.50 (m, 14H), 8.03 (s, 2H) (aromatic protons). ^{13}C (100 MHz, CDCl_3): δ 9.53,

Table 1
Selected bond lengths (Å), bond angles (°) and torsional angles (°) of **1**.

Bond lengths (Å)	Experimental XRD (Å)	Bond angles (°)	Experimental XRD (°)	Torsional angles (°)	Experimental XRD (°)
N1–C2	1.38(1.42)	C2–N1–C5	106.9(106.7)	C5–N1–C2–N3	–0.05(0.22)
N1–C5	1.84(1.41)	C2–N1–C11	128.6(127.7)	C5–N1–C2–C21	176.9(179.0)
N1–C11	1.44(1.41)	C5–N1–C11	123.3(125.4)	C11–N1–C2–N3	167.4(174.9)
N3–C2	1.32(1.36)	C2–N3–C4	106.5(106.4)	C11–N1–C2–C21	–15.60(–0.04)
N3–C4	1.37(1.40)	N1–C2–N3	110.5(110.8)	C2–N1–C5–C4	0.51(0.212)
C2–C21	1.46(1.46)	N1–C2–C21	126.4(124.6)	C2–N1–C5–C51	178.2(179.9)
C4–C5	1.36(1.42)	N3–C2–C21	123.0(124.6)	C11–N1–C5–C4	–167.8(175.0)
C4–C41	1.50(1.47)	N3–C4–C5	110.2(110.0)	C11–N1–C5–C51	10.9(5.03)
C5–C51	1.49(1.47)	N3–C4–C41	121.4(123.7)	C2–N1–C11–C12	117.6(133.4)
C11–C12	1.38(1.41)	C5–C4–C41	128.4(126.3)	C2–N1–C11–C16	–64.96(47.9)
C11–C16	1.38(1.41)	N1–C5–C4	105.9(106.1)	C5–N1–C11–C12	–76.77(52.9)
C12–C13	1.39(1.39)	N1–C5–C51	122.5(128.7)	C5–N1–C11–C16	100.7(126.2)
C13–C14	1.39(1.40)	C4–C5–C51	131.6(128.7)	C4–N3–C2–N1	–0.43(0.138)
C14–C15	1.38(1.40)	N1–C11–C12	119.8(120.3)	C4–N3–C2–C21	177.6(178.2)
C15–C16	1.39(1.41)	N1–C11–C16	119.2(120.8)	C2–N3–C4–C5	–0.77(0.00)
C21–C22	1.39(1.40)	C12–C11–C16	121.0(119.0)	C2–N3–C4–C41	178.0(179.2)
C21–C26	1.40(1.40)	C11–C12–C13	119.1(120.1)	N1–C2–C21–C22	–18.3(43.67)
C22–C23	1.39(1.39)	C12–C13–C14	121.2(120.9)	N1–C2–C21–C26	164.9(138.8)
C23–C24	1.32(1.41)	C13–C14–C15	118.3(119.0)	N3–C2–C21–C22	158.3(134.1)
C25–C26	1.38(1.39)	C14–C15–C16	121.5(122.0)	N3–C2–C21–C26	–18.4(43.36)
F4–C24	1.36(1.35)	C11–C16–C15	119.0(118.9)	N3–C4–C5–N1	–0.79(0.136)
		C2–C21–C22	124.2(120.9)	N3–C4–C5–C51	–179.3(179.3)
		C2–C21–C26	117.7(119.2)	C41–C4–C5–N1	–177.9(–179.0)
		C22–C21–C26	118.0(119.9)	C41–C4–C5–C51	–0.57(1.560)
		C21–C22–C23	121.2(120.4)	N1–C11–C12–C13	–177.0(179.4)
		C22–C23–C24	118.7(119.5)	C16–C11–C12–C13	–0.3(0.210)
		C23–C24–C25	122.1(122.2)	N1–C11–C16–C15	177.5(179.6)
		C24–C25–C26	118.7(119.6)	C12–C11–C16–C15	–0.1(0.530)
		C21–C26–C25	121.3(120.4)	C11–C12–C13–C14	0.5(0.075)
				C13–C14–C15–C16	–0.02(0.017)
				C17–C14–C15–C16	178.5(179.4)
				C14–C15–C16–C11	0.4(0.351)
				C2–C21–C22–C23	–177.2(178.3)
				C2–C21–C26–C25	–177.3(–178.3)
				F4–C22–C23–C24	179.8(179.5)
				F4–C24–C25–C26	179.7(179.9)

Values in the parenthesis are corresponding to the theoretical values.

55.1 115.25, 125.05, 126.47, 127.50, 127.69, 128.68, 129.69 130.45, 145.61. MS: m/z 416.00, calcd. 416.19.

2.3.9. 4-(4,5-Diphenyl-1-p-tolyl-1H-imidazol-2-yl)phenol (**6**)

Yield: 58%. Mp 231 °C, Anal. Calcd. For $C_{28}H_{22}N_2O$: C, 83.56; H, 5.51; N, 6.96. Found: C, 82.58; H, 5.23; N 6.56. FTIR (cm^{-1}) 1245, 1542, 1635, 2876, 3589, 3721. 1H NMR (400 MHz, $CDCl_3$): δ 2.20 (s, 3H), 6.93 (d, 2H), 7.53–7.89 (m, 14H), 7.92 (d, 2H), 12.52 (brs, 1H) (aromatic protons). ^{13}C (100 MHz, $CDCl_3$): δ 9.52, 113.20, 119.76, 125.01, 127.50, 127.69, 130.45, 144.78, 158.30 MS: m/z 402.00, calcd. 402.70.

3. Results and discussion

3.1. Steric hindrance in imidazoles: X-ray analysis

X-ray data of (**1**) (Table 1) reveal that the imidazole ring is essentially planar [18] and makes dihedral angles of 72.33° and 18.71° with the methylphenyl and fluorophenyl rings, respectively. The dihedral angle between the two benzene rings is 75.05° (Fig. 1). The crystal packing is stabilized by intermolecular C–H(N hydrogen bonds). The crystal packing is stabilized by C12–H12(N3 ($2-x$, $1-y$, $-z$) and C16–H16(N3 ($2-x$, $2-y$, $-z$) intermolecular hydrogen bonds (Table 2, Fig. 2). In order to eliminate crystal packing effect in the solid state, the molecular geometry of **1–6** is further examined by DFT calculation [15] to make necessary comparison. Three key twists, designated as α , β and γ have been examined. α is used to indicate the twist of imidazole ring from the aromatic six-membered ring at C(2), β and γ are used for twists of imidazole

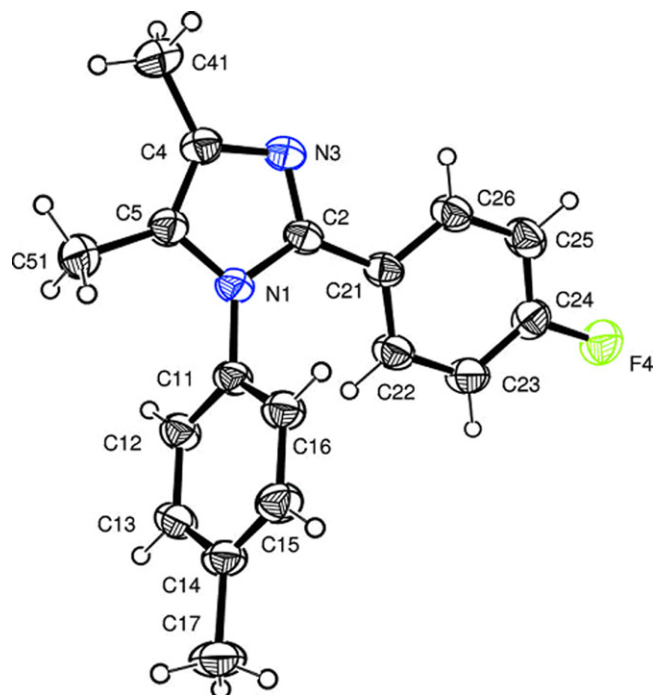


Fig. 1. Ortep diagram of (**1**).

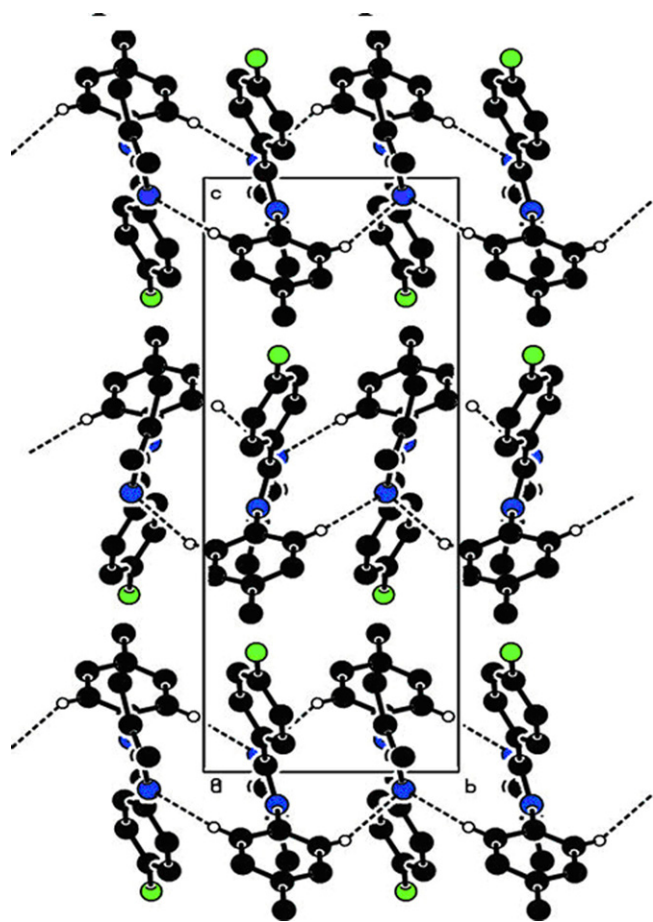


Fig. 2. The packing of fpdmti (1) viewed down the *a* axis. Dashed lines indicate hydrogen bonds. H atoms not involved in hydrogen bonding have been omitted.

Table 2
Hydrogen-bond geometry (Å) of 1.

D–H...A	D–H	H...A	D(A)	D–H...A
C12–H12...N3	0.93	2.55	3.3714	148
C16–H16...N3	0.93	2.60	3.5154	167

ring from phenyls at C(5) and C(4) positions, respectively (Fig. 3). By comparison of results in Table 3 several additional interesting structural features can be concluded that the γ twist is always smaller than the β twist. The β twist originates from the interaction of substituent at N(1) of the imidazole with the methyl group at C(5) whereas the γ twist is a result of the interaction of the methyl group at C(4) with the other one at C(5). The β twist always increases upon the substitution at N(1) of the imidazole derivatives compared to the parent counterparts and the substitution increases the β twist but decreases the γ twist. The present structural information allows us to further explore the correlation between structural features and fluorescent property. It reveals that α twist is corre-

Table 3
Deviation parameters ($^\circ$) of imidazole from other rings.

Compound	(α)	(β)	(γ)
1	-43.68	5.03	-179.02
2	42.16	-2.12	-178.87
3	-21.90	1.49	-179.22
4	-89.62	-5.08	-179.03
5	-139.70	-2.12	-178.87
6	42.16	-2.12	-178.87

lated with fluorescent property, the larger the α twist, the more drop the fluorescence quantum yield. Such a clear correlation indicates the importance of coplanarity between imidazole and the aromatic ring at C(2). This correlation can be ascribed to the conjugation rigidity. When the two adjacent aromatic species are in a coplanar geometry, the p-orbitals from the C–C bond connecting the two species will have maximal overlapping and the two rings will have a rigid and delocalized conjugation, as the result, the bond is no longer a pure single bond, as evident from the X-ray data of (1). The present bond distance of C2–C21 is 1.464(4) Å (Table 1) is shorter than the regular single bond distance between two sp^2 carbons (1.48 Å) [18], because of delocalization. When the two rings are deviated from each other, the p-orbital overlapping will be reduced. All these XRD data are in good agreement with the theoretical values. However, from the theoretical values it can be found that most of the optimized bond lengths, bond angles and dihedral angles are slightly higher than that of XRD values. These deviations can be attributed to the fact that the theoretical calculations were aimed at the isolated molecule in the gaseous phase whereas the XRD results were aimed at the molecule in the solid state.

3.2. Second harmonic generation (SHG) studies of 1–6

Second harmonic signal of 50 mV, 48 mV, 85 mV, 70 mV, 69 mV and 40 mV was obtained for 1–6 by an input energy of 4.1 mJ/pulse. But the standard KDP crystal gave a SHG signal of 110 mV/pulse for the same input energy. The second order nonlinear efficiency will vary with the particle size of the powder sample [19]. Higher efficiencies are achieved by optimizing the phase matching [20]. On a molecular scale, the extent of charge transfer (CT) across the NLO chromospheres determine the level of SHG output, the greater the CT and the larger the SHG output.

3.3. Comparison of $\mu\beta_0$

The overall polarity of the synthesized imidazole derivatives is small when their dipole moments aligned in a parallel fashion (Fig. 4). When the electric field is removed, the parallel alignment of the molecular dipole moments begins to deteriorate and eventually the imidazole derivatives loses its NLO activity. The ultimate goal in the design of polar materials is to prepare compounds which have their molecular dipole moments aligned in the same direction [21].

Theoretical investigation can play an important role in understanding structure–property relationship, which is able to assist in designing novel NLO chromophores. The electrostatic first hyperpolarizability (β) and dipole moment (μ) of the imidazole chromophores have been calculated by using Gaussian 03 package [14]. From Table 4, it is found that all the imidazole chromophores show larger $\mu_g\beta_0$ values, which is attributed to the positive contribution of their conjugation. The chromophore 3 exhibits larger nonlinearity than other chromophores and its λ_{\max} is red-shifted. Therefore, it is clear that the hyperpolarizability is a strong function of the absorption maximum. Since even a small absorption at the operating wavelength of optic devices can be detrimental, it is important to make NLO chromophores as transparent as possible without compromising the molecule's nonlinearity. Thermal stability of the imidazole chromophores was estimated by thermo gravimetric analysis (TGA). All samples show appreciable decomposition temperature (T_d) and their iridium complexes are ideal candidates for device application [21–23].

To determine the transference region and hence to know the suitability of these compounds (1–6) for microscopic nonlinear optical applications, the UV–visible spectra have been recorded by using the spectrometer in the range of 190–1100 nm. These

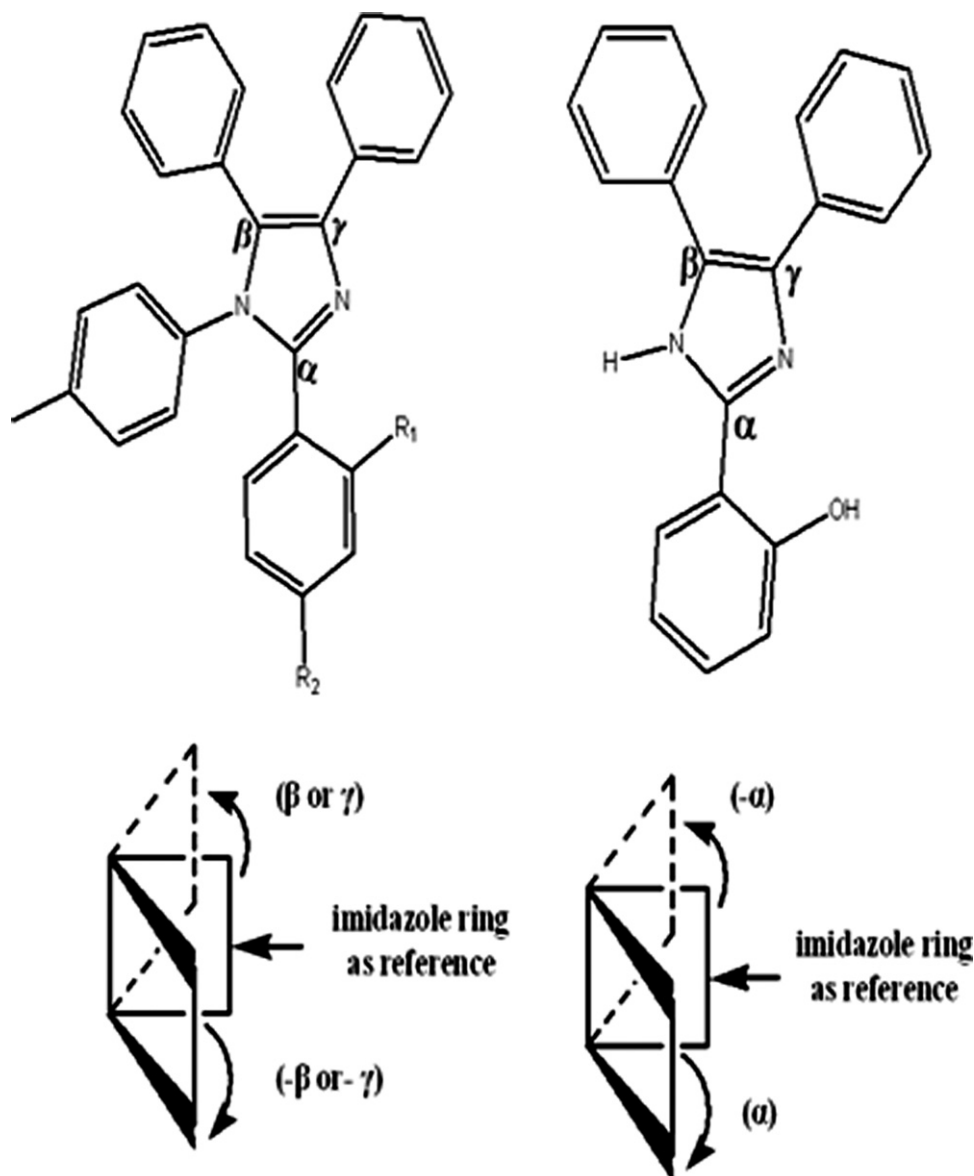


Fig. 3. Schematic presentation of α , β , and γ .

compounds show absorption spectra in the UV region between 238 and 303 nm. The increased transparency in the visible region might enable the microscopic NLO behavior with non-zero values [24–26]. All the absorption bands are due to $\pi \rightarrow \pi^*$ transitions. The β values (Table 5) computed here might be correlated with UV–visible spectroscopic data in order to understand the molecular-structure and NLO relationship in view of a future optimization of the microscopic NLO properties. The band at around 303.9 nm exhibits a solvatochromic shift, characteristic of a large dipole moment and frequently suggestive of a large hyperpo-

larizability. These compounds show red shift in absorption with increasing solvent polarity, accompanied with the upward shifts non-zero values in the β -components.

3.4. Octupolar and dipolar components of three types of chromophores

These chromophores possess a more appropriate ratio of off-diagonal versus diagonal β tensorial component ($r = \beta_{\beta_{xyy}} / \beta_{xxx}$) which reflects the inplane nonlinearity anisotropy and the largest

Table 4
Characterization of chromophores 1–6.

Chromophore	λ_{\max} (nm)	$(g \text{ (D)})$	$\beta_0/10^{-30}$ (esu)	$(g\beta_0/10^{-48}$ (esu)	T_d ($^{\circ}\text{C}$)	r	ρ
1	290.5	2.848	62.759	078.7	336	−0.03	0.42
2	291.5	2.092	40.353	68.2	348	−0.05	0.43
3	303.9	4.838	85.292	412.6	275	−0.002	0.34
4	248.0	3.513	68.028	239.0	360	0.03	0.26
5	238.0	2.886	65.248	188.3	312	0.04	0.24
6	245.0	2.022	23.039	46.6	282	0.03	0.25

Table 5
Electric dipole moment (D), polarizability (α) and Hyperpolarizability (β_{total}) of **1–6** calculated using B3LYP/6-31G(d,p).

Parameter	1	2	3	4	5	6
Dipole moment (D)						
μ_x	0.989	0.644	2.256	0.6248	0.586	0.489
μ_y	2.985	-0.2193	1.580	2.829	-1.278	2.249
μ_z	-1.126	1.667	1.002	1.308	3.578	-0.716
μ_{total}	2.848	2.092	4.838	3.513	2.886	2.022
Polarizability (α)						
α_{xx}	264.263	356.011	332.008	397.513	404.677	407.74
α_{xy}	13.329	-17.764	-2.059	-5.407	-6.956	-4.441
α_{yy}	112.687	181.969	113.913	205.714	218.053	202.304
α_{xz}	0.799	0.706	7.612	-20.559	-18.396	-17.275
α_{yz}	4.861	20.134	44.206	2.476	-2.989	8.552
α_{zz}	262.696	355.967	261.482	364.633	380.292	360.502
$\alpha \times 10^{-24}$ (esu)	28.634	44.161	34.945	47.812	49.549	47.945
Hyperpolarizability						
β_{xxx}	736.149	-234.895	1467.095	1274.941	1235.909	674.220
β_{xxy}	-43.675	-71.618	17.143	10.089	-14.388	11.716
β_{xyy}	-19.818	12.649	-3.778	36.845	47.367	22.592
β_{yyy}	3.327	-79.295	-1.530	32.446	11.864	7.766
β_{xxz}	91.762	-23.718	28.022	168.783	188.955	128.571
β_{xyz}	-3.221	20.984	61.696	-30.499	-17.898	-0.123
β_{yyz}	-37.747	-14.618	-2.350	-56.724	-57.310	-31.647
β_{xzz}	2.624	-93.660	-481.147	-537.059	-537.119	-556.211
β_{yzz}	49.597	1.662	23.894	29.728	49.598	9.054
β_{zzz}	-285.077	-24.900	-117.661	-232.961	-238.553	-143.166
$\beta \times 10^{-31}$ (esu)	62.759	40.353	85.292	68.028	65.247	23.039

esu: electrostatic unit; (1 a.u. = 8.3693×10^{-33} e.s.u.); x, y, z: principle axis.

$\mu\beta_0$ values. The difference of the β_{xyy}/β_{xxx} ratios for these chromophores can be well understood by analyzing their relative molecular orbital properties. The electrostatic first hyperpolarizabilities (β_0) and dipole moment (μ) of the chromophores have been investigated theoretically and it is found that the ground state dipole moments of the six chromophores are in the order $\mu(3) > \mu(4) > \mu(5) > \mu(1) > \mu(6) > \mu(2)$ and this can be well understood by the vector additive model. The sequence of their β_0 values are in the order of $\beta_0(3) > \beta_0(4) > \beta_0(5) > \beta_0(1) > \beta_0(6) > \beta_0(2)$. This

observed sequence can be explained by the reduced planarity in such chromophores caused by the steric interaction between the two phenyl rings at C(2) and N(4) atoms. Hence, the steric interaction must be reduced in order to obtain larger β_0 values.

The β tensor [25] can be decomposed in a sum of dipolar (${}^2D_{j=1}\beta$) and octupolar (${}^2D_{j=3}\beta$) tensorial components, and the ratio of these two components strongly depends on their 'r' ratios. The zone for $r > r_2$ and $r < r_1$ corresponds to a molecule of octupolar and dipolar respectively. The critical values for r_1 and r_2 are $(1 - \sqrt{3})/\sqrt{3}(\sqrt{3}+1) = -0.16$ and $(\sqrt{3}+1)/\sqrt{3}(\sqrt{3}-1) = 2.15$, respectively. Complying with the Pythagorean theory and the projection closure condition, the octupolar and dipolar components of the β tensor can be described as:

$$\|{}^2D_{j=1}\beta\| = \frac{3}{4}[(\beta_{xxx} + \beta_{xyy})^2 + ((\beta_{yyy} + \beta_{yxx})^2)] \quad (5)$$

$$\|{}^2D_{j=3}\beta\| = \frac{1}{4}[(\beta_{xxx} + 3\beta_{xyy})^2 + ((\beta_{yyy} + \beta_{yxx})^2)] \quad (6)$$

The parameter $\rho^{2D}[\rho^{2D} = (\|{}^2D_{j=3}\beta\|)/(\|{}^2D_{j=1}\beta\|)]$ is convenient to compare the relative magnitudes of the octupolar and dipolar components of β . The observed positive small ρ values (Table 4) of imidazole derivatives reveal that the β_{iii} component cannot be zero and these are dipolar component. Since most of the practical applications for second order NLO chromophores are based on their dipolar components, this strategy is more appropriate for designing highly efficient NLO chromophores.

3.5. Bond length and occupation coefficient for quantifying the push-pull effect in imidazoles

The two push-pull parameters [bond lengths d (Å) and occupation quotients π^*/π] of the partial C=N and C=C bonds of the linking chain N=C-C=C were calculated (Table 6) and the corresponding values are correlated in Fig. 5. The linear correlation indicate that with increasing donor-acceptor character of the imidazoles **1–6** the two partial C=N and C=C bonds are elongated, thereby the occupation quotients π^*/π increased. Thus the imidazoles can be confirmed to be strongly polarized, π -delocalized materials which should exhibit NLO behavior.

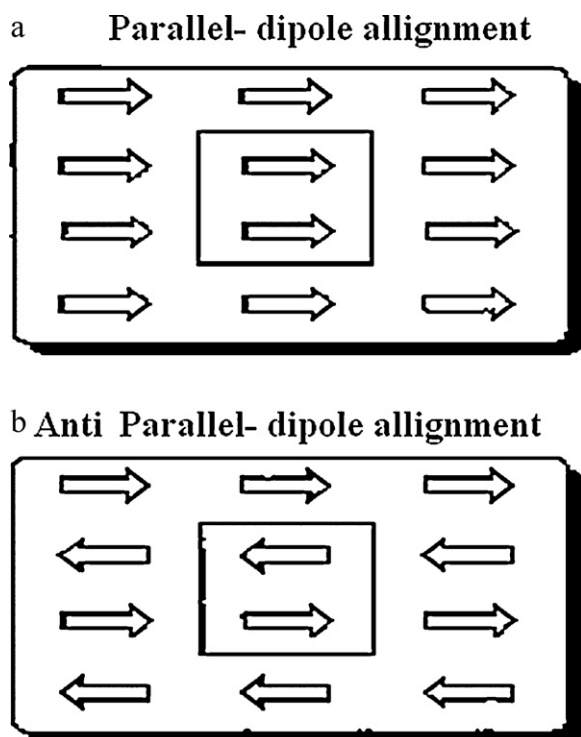


Fig. 4. Orientation of dipole moments.

Table 6

Occupation numbers of antibonding π^* and bonding π orbitals of the corresponding partial C=N and C=C double bonds, molecular hyperpolarizability (β_0) and dipole moments (μ) of **1–6**.

Compound	π	π^*	π^*/π	d (Å)	$\sigma\pi^*/\pi/2$
1	1.670	0.363	0.217	1.356	0.189
2	1.653	0.364	0.220	1.254	0.151
3	1.641	0.395	0.241	1.263	0.233
4	1.654	0.369	0.223	1.324	0.207
5	1.681	0.350	0.208	1.362	0.191
6	1.971	0.019	0.010	1.215	0.008

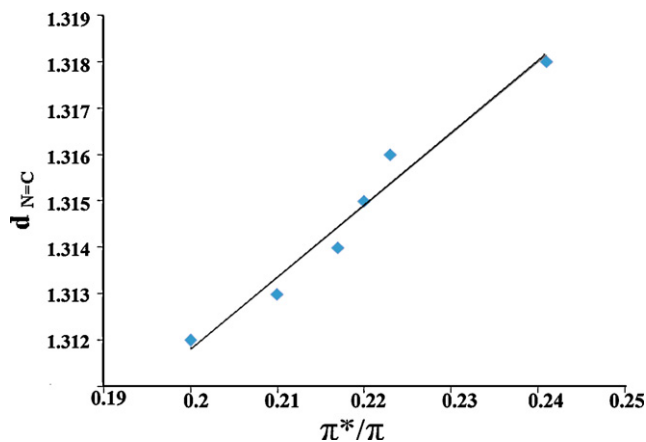


Fig. 5. Correlation of bond length (Å) and occupation co-efficient.

These two parameters [bond lengths $d_{N=C}$ (Å) and occupation quotients π^*/π] quantifying the donor–accepter properties of the studied imidazoles, the molecular hyperpolarizability have been correlated with the mean of the sum of π^*/π N=C and the π^*/π C=C quotients. A clear linear dependence (Fig. 6) of the two parameters shows that, the polarity of these compounds for potential application as NLO material is important, but not deciding. Molecules of higher hyperpolarizability have larger dipole moments used as potential NLO molecules (characterized by bond lengths, occupation p^*/p quotients and dipole moment variations) [25].

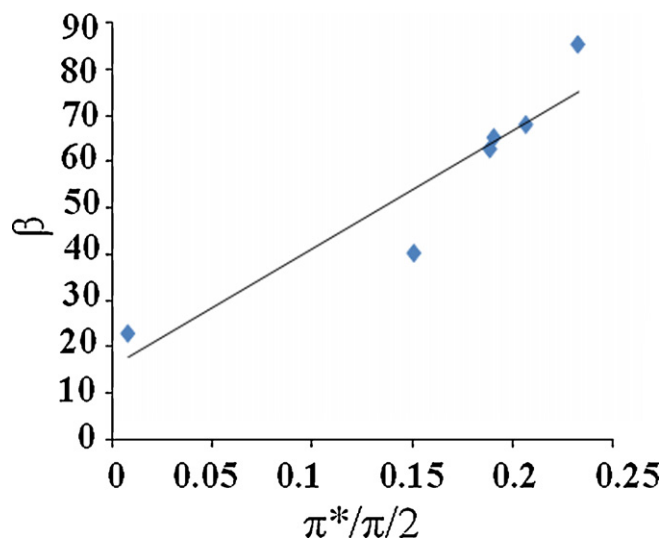


Fig. 6. Correlation of molecular hyper polarizability and mean of the sum of occupation co-efficient.

3.6. Natural Bond Orbital (NBO) analysis

NBO analyses have been performed for **1–6** at the DFT/B3LYP/6-31++G(d,p) level in order to elucidate the intramolecular, hybridization and delocalization of electron density within the molecule. The intramolecular interactions are formed by the orbital overlap between σ (C–C) and σ^* (C–C) bond orbital which results intramolecular charge transfer (ICT) causing stabilization of the system. These interactions are observed as increase in electron density (ED) in C–C antibonding orbital that weakens the respective bonds [27].

The importances of hyperconjugative interaction and electron density transfer (EDT) from lone pair electrons to the antibonding orbital have been analyzed and the results [28] are presented in Tables 7 and 8. Several donor–acceptor interactions are observed in **1** and among the strongly occupied NBOs, the most important delocalization sites are in the π system and in the lone pairs (n) of the oxygen, fluorine and nitrogen atoms of **1**. The σ system shows some contribution to the delocalization, and the important contributions to the delocalization corresponds to the donor–acceptor interactions are C6–C10 \rightarrow C15–C19, C16–C19 \rightarrow C6–C10, C17–H20 \rightarrow C15–C16, C18–H22 \rightarrow C17–H20, C18–H22 \rightarrow C17–H20, C27–C28 \rightarrow C29–C32, C29–C32 \rightarrow C30–C34, C30–C34 \rightarrow C27–C28, C40–C43 \rightarrow C41–C45, C41–C45 \rightarrow C38–C39, C29–C32 \rightarrow C30–C34 and C29–C32 \rightarrow C30–C34

The charge distribution of **1** was calculated by the NBO and Mulliken methods (Fig. 7). These two methods predict the same tendencies *i.e.*, among the nitrogen atom N4 and N5, N5 is considered as more basic site [29]. The charge distribution shows that the more negative charge is concentrated on N5 atom whereas the partial positive charge resides at hydrogens.

3.7. Vibrational assignments

The molecule (**1**) has 38 atoms and hence can have 108 normal modes of vibrations. According to the molecule possess a non-planar structure with C1 point group symmetry. The observed FT-IR and various modes of frequencies are calculated theoretically. Only few selected vibrations are discussed and displayed in Table 9 (Fig. 8a and b).

3.7.1. O–H vibrations

In the case of alcohols a very sharp band appears around 3600 cm^{-1} in very dilute solution using non-polar solvents if intramolecular hydrogen bonding is absent [30]. In bonded form, a broad and intense band appears in the region $3200\text{--}3550\text{ cm}^{-1}$. In the present work the broad band centered at 3427 cm^{-1} is assigned to O–H stretching modes for **4** and **6**. The calculated theoretical OH vibrations after scaling are in good agreement with experimental vibrations.

3.7.2. C–H vibrations

Presence of band in the region $2700\text{--}3000\text{ cm}^{-1}$ is the characteristic region for the identification of C–H stretching vibrations

Table 7
Significant donor–acceptor interactions of (1) and their second-order perturbation energies (kcal/mol).

Donor (<i>I</i>)	Type	ED/e	Acceptor (<i>J</i>)	Type	ED/e	$E(2)$ a.u	$E(j)-E(i)$	$F(I, j)$
C1–C2(2)	π	1.81,620	C3–N5(2)	π^*	0.41,502	12.51	0.26	0.054
C3–N5(2)	π	1.83,922	C1–C2(2)	π^*	0.30,914	20.06	0.33	0.075
C6–C8(2)	π	1.64,093	C3–N5(2)	π^*	0.41,502	18.28	0.25	0.062
C6–C8(2)	π	1.64,093	C7–C9	π^*	0.30,942	20.15	0.28	0.068
C6–C8(2)	π	1.64,093	C10–C11	π^*	0.38,650	20.54	0.26	0.066
C7–C9(2)	π	1.69,281	C6–C8(2)	π^*	0.39,486	16.92	0.28	0.063
C7–C9(2)	π	1.69,281	C10–C11(2)	π^*	0.38,650	21.06	0.26	0.068
C10–C11(2)	π	1.65,543	C6–C8(2)	π^*	0.39,486	21.14	0.29	0.071
C10–C11(2)	π	1.65,543	C7–C9(2)	π^*	0.30,944	16.61	0.29	0.063
C23–C25(2)	π	1.67,726	C24–C26(2)	π^*	0.31,091	18.88	0.29	0.066
C23–C25(2)	π	1.67,726	C28–C30(2)	π^*	0.33,506	18.35	0.29	0.06
C24–C26(2)	π	1.68,388	C23–C25(2)	π^*	0.037,815	19.24	0.27	0.066
C24–C26(2)	π	1.68,388	C28–C30(2)	π^*	0.33,506	20.03	0.29	0.068
C28–C30(2)	π	1.65,174	C23–C25(2)	π^*	0.37,815	22.18	0.27	0.069
C28–C30(2)	π	1.65,174	C24–C26(2)	π^*	0.31,091	19.01	0.28	0.065
LP(1)N4	σ	1.57,526	C1–C2(2)	π^*	0.30,914	27.48	0.30	0.084
LP(1)N5	σ	1.93,041	C3–N5(2)	π^*	0.41,502	43.07	0.26	0.095
LP(1)N4	σ	1.96,627	C23–C25(2)	π^*	0.37,815	14.62	0.27	0.056
LP(3)F34	π	1.91,538	C10–C11(2)	π^*	0.38,650	20.16	0.42	0.089

Table 8
Percentage of s and p-character on each natural atomic hybrid of the Natural Bond Orbital.

Bond (A–B)	E_D/Energy (a.u.)	$ED_A\%$	$ED_B\%$	NBO	s%	p%
C1–C2(2)	0.7149	51.10	48.90	0.715(sp ^{1.00})	0.00	99.93
	0.6993	–	–	0.700(sp ^{1.00})	0.00	99.92
C6–C8(2)	0.7131	50.85	49.15	0.713(sp ^{1.00})	0.01	99.97
	0.7011	–	–	0.701(sp ^{1.00})	0.01	99.95
C6–C8(2)	0.7006	49.08	50.92	0.701(sp ^{1.00})	0.00	99.95
	0.7136	–	–	0.714(sp ^{1.00})	0.00	99.96
C7–C9(2)	0.7075	50.06	49.94	0.708(sp ^{1.00})	0.00	99.96
	0.7067	–	–	0.707(sp ^{1.00})	0.00	99.96
C10–C11(2)	0.7221	52.15	47.85	0.722(sp ^{1.00})	0.00	99.97
	0.6918	–	–	0.692(sp ^{1.00})	0.00	99.95
C23–C25(2)	0.7027	49.38	50.62	0.703(sp ^{1.00})	0.00	99.95
	0.7115	–	–	0.712(sp ^{1.00})	0.00	99.96
C24–C26(2)	0.7148	51.09	48.91	0.715(sp ^{1.00})	0.00	99.96
	0.6993	–	–	0.700(sp ^{1.00})	0.00	99.95
C28–C30(2)	0.6463	41.77	58.23	0.646(sp ^{2.03})	33.00	66.95
	0.7631	–	–	0.763(sp ^{1.71})	36.80	62.98

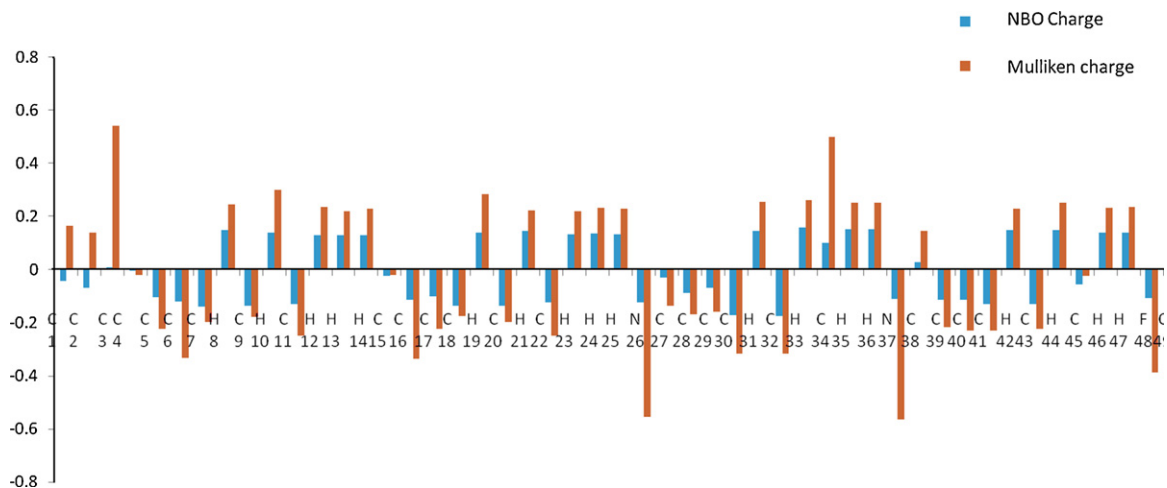


Fig. 7. Bar diagram of NBO charge versus Mulliken charges.

Table 9

Vibrational assignments of 2-(4-fluorophenyl)-4,5-dimethyl-1-p-tolyl-1H-imidazole (**1**) at B3LYP/6-31G(d,p), HF/6-31G(d,p) and HF/6-311G(d,p) [harmonic frequency (cm^{-1}), IR, Raman intensities (Km/mol^{-1}), reduced masses (amu), force constants ($\text{mdyn}\text{\AA}^{-1}$)].

Sl. no	Calculated frequencies (cm^{-1})			HF6-311G(d,p)		HF6-311G(d,p)		Vibrational assignment
	B3LYP/6-31G(d,p)	HF/6-31G(d,p)	HF/6-311G(d,p)	Intensity	Activity	Reduced mass	Force constant	
1	25	56	57	0.1	1.1	5.7603	0.0134	τ -torsion sub CH3 in Im
2	28	82	83	0.2	0.0	4.3289	0.0216	τ -torsion
3	42	88	89	0.3	0.2	3.7603	0.0216	τ -torsion
4	45	106	109	0.1	1.6	3.8690	0.0331	τ -torsion
5	63	114	116	0.1	0.3	4.2220	0.0410	τ -torsion
6	64	131	133	0.6	2.9	4.1241	0.0526	τ -torsion
7	76	163	164	0.4	0.3	4.7156	0.0909	τ -torsion of sub CH3 in Im
8	101	188	189	0.9	0.2	4.7124	0.1209	τ -torsion
9	139	216	217	0.4	0.9	3.7642	0.1274	τ -torsion of sub CH3 in Im
10	152	227	225	1.2	0.9	2.1288	0.0775	τ -torsion of sub CH3 in Im
11	168	251	250	0.6	0.5	2.4846	0.1119	ω -C7-C27 + ω -C4-C35 + ω -C5-C31
12	193	259	258	1.0	0.3	2.2293	0.1064	ω -C4-C35 + ω -C5-C31
13	231	276	272	0.3	0.2	1.0717	0.0571	ω -C4-C35 + ω -C5-C31 + ω -C1-C16
14	247	286	286	0.7	0.2	3.2503	0.1913	δ -C4-C35 + δ -C5-C31
15	280	299	300	1.7	0.9	4.0932	0.2642	ω -C-H of Ph1 and Im
16	289	319	319	0.3	0.9	1.9016	0.1393	δ -C4-C35 + δ -C5-C31 + δ -C7-C27
17	309	332	332	0.3	0.5	1.8405	0.1459	δ -C4-C35 δ -C7-C27
18	335	357	358	2.0	1.9	2.7748	0.2555	ω -C-H of Ph1 and Im
19	352	372	373	0.4	1.2	4.2833	0.4285	ω -C-H of Ph1 + ω -C1-C16
20	364	386	388	0.5	1.6	4.8408	0.5235	ω -C-H of Ph1 + ω -C7-C27
21	405	420	422	0.7	0.6	4.7321	0.6058	ω -C=C of Ph1 and Ph2
22	405	441	443	0.1	0.4	3.9752	0.5607	ω -C=C of Ph1
23	408	444	445	0.3	0.5	3.9030	0.5570	ω -C=C of Ph1 and Ph2
24	430	446	448	0.1	0.4	3.1474	0.4535	ρ -C-H of Ph1
25	492	534	537	3.1	0.2	3.5720	0.7416	ω -C-H of Ph1
26	509	554	558	5.1	0.3	3.1677	0.7104	ω -C-H-C-H of Ph2
27	559	560	562	10.6	0.9	5.7285	1.3015	ρ -C=C of Ph1
28	572	575	577	4.1	0.5	5.4821	1.3111	ρ -C=C of Ph1 and Ph2
29	581	609	611	10.8	0.2	3.5932	0.9652	ω -C-H of Ph1 and Ph2
30	616	620	622	1.4	2.8	6.4517	1.7947	Ring breathing of Ph1 and Ph2
31	621	630	632	0.4	1.0	6.3223	1.8138	Ring breathing of Ph1 and Ph2
32	643	657	659	2.3	2.0	5.0130	1.5669	ω -C4-C5-N3
33	655	679	684	1.5	1.7	4.6861	1.5786	Ring breathing of Im
34	676	718	723	1.5	0.6	4.0190	1.5126	ω -C=C Ph2 + ω -N2-C1-N3
35	700	730	735	2.5	0.3	4.4320	1.7240	ω -C=C Ph1
36	702	751	753	4.8	6.1	4.4995	1.8334	ω -C=C Ph1 + ω -N2-C1-N3
37	741	761	765	4.9	3.8	6.5058	2.7412	ω -C-H of Im and Ph2
38	782	781	781	5.2	5.2	5.5465	2.4335	δ -C=C of Ph1
39	792	803	800	4.4	10.3	5.6627	2.6089	ω -C-H of Ph2
40	802	875	877	33.9	0.1	1.3579	0.7507	ω -C-H of Ph1 + ring breathing of Ph2
41	813	880	880	0.6	1.0	1.2332	0.6862	ω -C-H of Ph1 and Ph2
42	813	890	894	47.9	0.1	1.5227	0.8747	ω -C-H of Ph1
43	816	895	895	0.2	0.3	1.2253	0.7063	ω -C-H of Ph1 and Ph2
44	910	938	938	12.6	10.7	4.5521	2.8797	ω -C-H of Ph2
45	921	977	968	1.7	0.5	2.5711	1.7335	ω -C-H of Ph1
46	928	978	978	0.1	5.7	2.3870	1.6422	ω -C-H of Ph1
47	931	993	992	1.3	0.9	2.6680	1.8899	ω -C-H of Ph2
48	937	995	994	0.2	1.2	2.6450	1.8790	(t)-C-H of Im
49	961	998	997	2.7	1.4	1.4767	1.0552	δ -C1-N2-C4
50	967	1001	1001	0.8	0.2	1.4014	1.0092	(t)-C-H of Ph1
51	983	1012	1002	0.6	2.2	2.7551	1.9892	δ -C=C of Im and Ph2
52	986	1021	1017	2.0	4.0	2.0936	1.5569	δ -C=C of Ph2
53	999	1021	1024	0.5	0.4	1.3510	1.0184	ρ -C-H of Ph1
54	1014	1022	1024	0.0	0.3	1.3211	0.9971	(t)-C-H of Im
55	1018	1043	1038	1.2	0.0	1.8670	1.4462	ω -C-H of Ph1
56	1022	1059	1060	0.4	0.5	1.3707	1.1078	ω -C-H of Im
57	1075	1073	1073	7.2	1.9	2.7189	2.2527	δ -C-H of Ph2
58	1087	1076	1077	2.4	0.6	1.6438	1.3718	δ -C-H of Ph1
59	1093	1080	1083	0.5	0.1	1.4839	1.2519	Ring breathing of Ph2
60	1117	1120	1116	4.5	1.0	2.0967	1.8771	ω -C-H of Im
61	1133	1131	1130	3.6	7.8	2.5829	2.3719	δ -C-H of Ph2
62	1152	1153	1153	12.4	2.7	1.2003	1.1474	δ -C-H of Ph1
63	1181	1158	1155	2.1	3.3	1.7622	1.6901	ν -C7-C27 + δ C=C of Ph1
64	1223	1175	1175	0.0	1.3	1.2465	1.2372	ν -C-F + ρ -C-H of Ph2
65	1228	1197	1194	24.6	11.3	3.5100	3.5994	δ -N2-C4-C5
66	1263	1213	1205	66.9	2.9	3.6622	3.8248	ρ -C-H of Ph2
67	1270	1224	1215	41.9	21.2	3.2355	3.4372	ρ -C-H of Ph1
68	1275	1263	1262	6.9	6.4	4.7318	5.4177	δ -C=C of Ph2
69	1281	1297	1298	1.6	1.1	1.3832	1.6765	ρ -C-H of Ph1
70	1285	1316	1316	13.5	4.4	1.5598	1.9426	δ -N2-C1-N3
71	1328	1324	1325	100.0	17.8	3.0529	3.8528	Ring deformation of Im (ν -C-N + ν -C=N)

Table 9 (Continued)

Sl. no	Calculated frequencies (cm ⁻¹)			HF6-311G(d,p)		HF6-311G(d,p)		Vibrational assignment
	B3LYP/6-31G(d,p)	HF/6-31G(d,p)	HF/6-311G(d,p)	Intensity	Activity	Reduced mass	Force constant	
72	1355	1376	1374	10.1	3.7	2.2918	3.1112	ν -C6-N3
73	1364	1389	1388	31.9	14.8	2.5204	3.4900	ν -C7-C27
74	1370	1397	1394	4.7	3.2	2.2077	3.0861	ν -C4-C35
75	1375	1409	1407	3.2	15.4	1.3907	1.9788	ν -C5-C31
76	1384	1410	1408	0.3	3.4	1.2644	1.8040	δ -C-H of sub CH3 in Ph1
77	1392	1427	1426	22.1	40.2	1.9456	2.8467	ν -C6-N3 + ν -C1-N3
78	1423	1446	1445	24.9	34.8	1.9365	2.9075	δ -C-H of sub CH3 in Im
79	1427	1455	1456	4.4	4.8	1.1861	1.8091	δ -C-H of sub CH3 in Im
80	1434	1459	1459	3.6	3.4	1.1046	1.6901	δ -C-H of sub CH3 in Ph1
81	1436	1462	1463	7.9	4.7	1.0495	1.6149	δ -C-H of sub CH3 in Im
82	1438	1469	1510	1.3	1.7	1.1900	1.8475	δ -C-H of sub CH3 in Im + δ -C-H of sub CH3 in Ph1
83	1439	1469	1521	2.6	4.1	1.0693	1.6608	δ -C-H of sub CH3 in Im
84	1451	1474	1539	0.6	3.2	1.1275	1.7636	ν -C1-N2
85	1488	1512	1559	79.8	3.8	2.3822	3.9061	ν -C6-N3
86	1498	1524	1563	78.0	43.1	3.3839	5.6276	ν -C=C of Ph2 + ν -C1-N3 + ν -C1-C16
87	1554	1540	1598	6.4	6.8	5.7141	9.7293	ν -C=C of Ph1 + ν -C=C of Im
88	1564	1563	1602	8.1	1.5	5.6598	9.8899	ν -C=C of Ph2 + ν -C=C of Im
89	1568	1566	2792	2.4	1.5	5.4524	9.5793	ν -C=C of Ph1 and Ph2 + ν -C1-N2
90	1591	1601	2794	4.4	38.1	4.8182	8.8530	ν -C=C of Ph1 and Ph2
91	1593	1606	2843	19.9	69.6	5.1048	9.4180	ν -C=C of Ph1 and Ph2
92	2899	2787	2846	28.1	60.6	1.0357	5.8052	ν -C-H of sub CH3 in Im
93	2904	2789	2853	22.6	25.6	1.0376	5.8242	ν -C-H of sub CH3 in Ph1
94	2907	2791	2796	33.0	100.0	1.0376	5.8322	ν -C-H of sub CH3 in Im
95	2945	2837	2836	31.7	39.4	1.1018	6.3750	ν -C-H of sub CH3 in Im
96	2960	2840	2841	8.5	17.8	1.1009	6.3900	ν -C-H of sub CH3 in Im
97	2962	2843	2843	14.0	22.9	1.1025	6.4096	ν -C-H of sub CH3 in Ph1
98	2987	2846	2846	15.7	28.8	1.1034	6.4286	ν -C-H of sub CH3 in Im
99	2988	2853	2853	14.5	13.8	1.1021	6.4508	ν -C-H of sub CH3 in Ph1
100	2998	2856	2855	9.9	31.5	1.1019	6.4617	ν -C-H of sub CH3 in Im
101	3038	2910	2910	8.3	20.3	1.0908	6.6426	ν -C-H of Ph1 (asym)
102	3039	2911	2911	10.4	29.3	1.0912	6.6486	ν -C-H of Ph1 (asym)
103	3061	2919	2918	1.4	12.7	1.0923	6.6903	ν -C-H of Ph1 (sym)
104	3068	2923	2923	3.7	9.6	1.0917	6.7068	ν -C-H of Ph2 (asym)
105	3068	2932	2932	3.6	20.4	1.0960	6.7754	ν -C-H of Ph1 (sym)
106	3069	2944	2944	4.4	28.1	1.0945	6.8224	ν -C-H of Ph2 (asym)
107	3083	2949	2948	3.3	30.1	1.0957	6.8486	ν -C-H of Ph2 (asym)
108	3086	2950	2949	4.2	61.0	1.0954	6.8518	ν -C-H of Ph2 (sym)

ν - stretching; β - in-plane; γ - out-of-plane bending; ω - wagging; t - twisting; δ - scissoring; ρ - rocking; τ - torsion. B - broad; S - strong; m - medium; w - weak. Scale factors: 0.955 [B3LYP/6-31G(d,p)]; 0.8992 [HF/6-31G(d,p)]; 0.9051 [HF/6-311G(d,p)].

[31]. In this region the bands are slightly affected by the nature of the substituents. The scaled vibrations are around 2800 cm⁻¹. The experimental C-H vibrations are in good agreement with theoretical vibrations.

3.7.3. C-N vibrations

The identification of the C-N vibration is a very difficult task since mixing of several bands is possible in this region. Silverstein and Webster [30] assigned the C-N stretching absorption in the region 1382–1266 cm⁻¹ for aromatic amines. The C-N stretching mode is reported at 1368 cm⁻¹ for benzamide [31], at 1382 and 1307 cm⁻¹ for benzotriazole [32], at 1335, 1331 cm⁻¹ for 2,4-dinitrophenylhydrazide [33] and at 1316 and 1213 cm⁻¹ for morpholine-4-ylmethylthiourea [34]. In the present study, a weak band observed in the spectra around 1228 cm⁻¹ and these frequencies are in good agreement with theoretically computed values.

3.7.4. C=C vibrations

The benzene ring possesses six stretching vibrations, of which the four with the highest wave numbers occurring near 1600, 1580, 1490 and 1440 cm⁻¹ are good group vibrations [35]. With heavy substituents, the bands tend to shift to somewhat lower wave numbers and greater the number of substituents on the ring, broader the absorption regions. In the present paper, the strong band around

1380 cm⁻¹ (1–6) is assigned to C=C stretching mode. The calculated wave number for this fundamental mode is around 1400 cm⁻¹ by B3LYP method.

3.7.5. Methyl group vibrations

The band at 2991 cm⁻¹ is assigned to the CH₃ asymmetric stretching [36]. For the assignments of CH₃ group frequencies one can expect nine fundamentals to be associated with each CH₃ group, viz., the symmetrical stretching in CH₃ (CH₃ sym. stretching), asymmetrical stretching (i.e., in-plane hydrogen stretching mode), the symmetrical (CH₃ sym. deformation) and asymmetrical (CH₃ asy. deformation) deformation modes, the in-plane rocking (CH₃ *ipr*) and twisting *t*(CH₃) modes. In addition to that CH₃ ops, out-of-plane stretch and CH₃ opb, out-of-plane bending modes of the CH₃ group would be expected to be depolarized for asymmetry species.

The C-H stretching in methyl group occurs at lower frequencies than use of the aromatic ring (3100–3000 cm⁻¹). The asymmetric and symmetric stretching are observed around 2900 cm⁻¹ are attributed to CH₃ asymmetric stretching modes, theoretically scaled values by B3LYP method around 3000 cm⁻¹ assigned to asymmetric stretching vibration. The scale down values 2900 cm⁻¹ by B3LYP method for methyl symmetric stretching vibration shows good agreement with the recorded FT-IR spectra. Very strong band around 1030 cm⁻¹ have assigned to CH₃ asymmetric and sym-

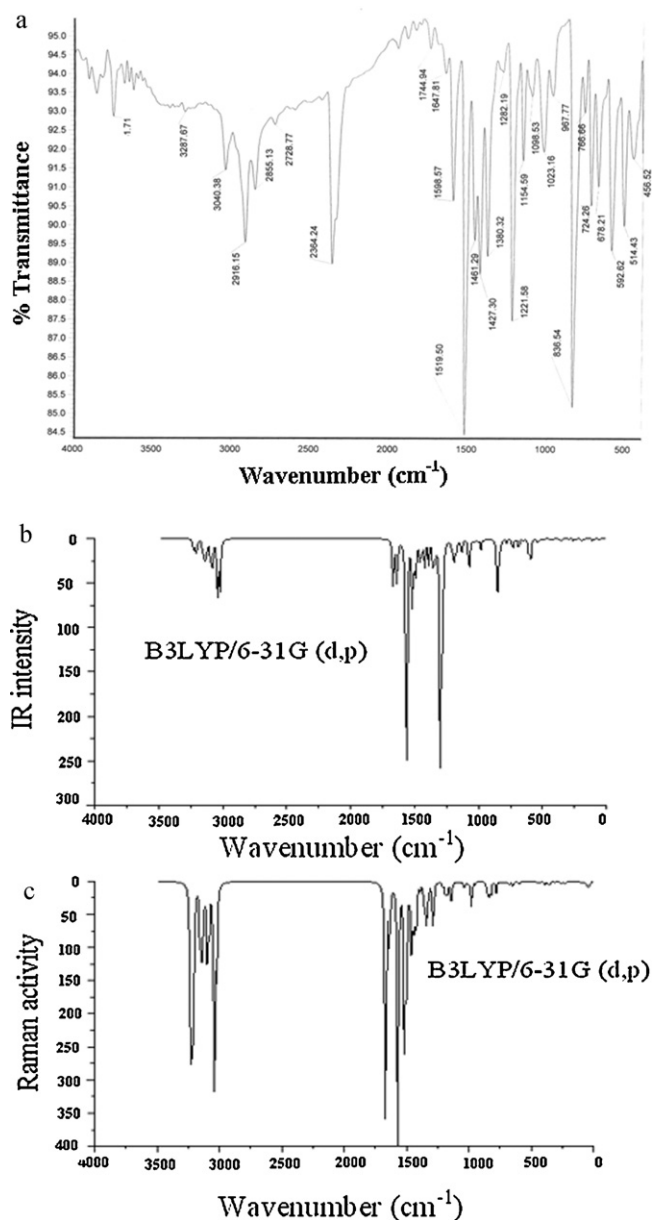


Fig. 8. (a) Experimental IR spectra of **1**. (b) Theoretical IR and Raman spectra of **1**.

metric deformations which are in satisfactory agreement with the theoretical values.

4. Conclusion

We have reported new simple and an efficient route to the synthesis of biologically active heterocycles, such as substituted imidazoles using iodine as the catalyst. The presence of α twist in these imidazoles drops the fluorescence quantum yield. The observed sequence of dipole moment and hyperpolarizability can be explained by the reduced planarity in these chromophores caused by the steric interaction between the two phenyl rings at C(2) and N(4) atoms. Hence, the steric interaction must be reduced in order to obtain larger β_0 values. A clear linear dependence of hyperpolarizability versus $\sigma \pi^*/\pi/2$ shows that the polarity of these compounds are important for potential application as NLO material. From the physicochemical studies on imidazoles it was concluded that molecules of higher hyperpolarizability have larger dipole moments used as potential NLO molecules.

Acknowledgments

One of the author Dr. J. Jayabharathi, associate professor in chemistry, Annamalai University is thankful to Department of Science and Technology [No. SR/S1/IC-07/2007] and University Grants commission (F. No. 36-21/2008 (SR)) for providing fund to this research work.

References

- [1] J.G. Lombardino, E.H. Wiseman, *J. Med. Chem.* 17 (1974) 1182–1188.
- [2] T. Maier, R. Schmierer, K. Bauer, H. Bieringer, H. Buerstell, B. Sachse, US Patent 820,335, Chem. Abstr. 111 (1989) 19494.
- [3] I. Lantos, W. Zhang, X. Shiu, D.S. Eggleston, *J. Org. Chem.* 58 (1993) 7092–7095.
- [4] C. Zhang, E.J. Moran, T.F. Woiwade, K.M. Short, A.M. Mjalli, *Tetrahedron Lett.* 37 (1996) 751–754.
- [5] S. Jianwei, Y. Dong, L. Cao, X. Wang, S. Wang, Y.Y. Hu, *J. Org. Chem.* 69 (2004) 8932–8934.
- [6] K. Mahalingam, M. Nethaji, P.K. Das, *J. Mol. Struct.* 378 (1996) 177–188.
- [7] R. Koch, J.J. Finnerty, T. Bruhn, *J. Phys. Org. Chem.* 21 (2008) 954–962.
- [8] G. Ye, W.P. Henry, C. Chen, A. Zhou, C.U. Pittman Jr., *Tetrahedron Lett.* 50 (2009) 2135–2139.
- [9] D.M. Mitchell, P.J. Morgan, D.W. Pratt, *J. Phys. Chem. A* 112 (2008) 12597–12601.
- [10] P. Rattanakin, C.U. Pittman Jr., W.E. Collier, S. Daeblo, *Struct. Chem.* 18 (2007) 399–407.
- [11] G. Fischer, W.D. Rudolf, E. Kleinpeter, *Magn. Reson. Chem.* 29 (1991) 204–206.
- [12] E. Kleinpeter, A. Schulenburg, *Tetrahedron Lett.* 46 (2005) 5995–5997.
- [13] E. Kleinpeter, A. Koch, B. Mikhova, B.A. Stamboliyska, T.M. Kolev, *Tetrahedron Lett.* 49 (2008) 1323–1327.
- [14] M.J. Frisch, G.W. Trucks, H.B. Schlegel, G.E. Scuseria, M.A. Robb, J.R. Cheeseman, J.A. Montgomery, T. Vreven Jr., K.N. Kudin, J.C. Burant, J.M. Millam, S.S. Iyengar, J. Tomasi, V. Barone, B. Mennucci, M. Cossi, G. Scalmani, N. Rega, G.A. Petersson, H. Nakatsuji, M. Hada, M. Ehara, K. Toyota, R. Fukuda, J. Hasegawa, M. Ishida, T. Nakajima, Y. Honda, O. Kitao, H. Nakai, M. Klene, X. Li, J.E. Knox, P. Hratchian, J.B. Cross, C. Adamo, J. Jaramillo, R. Gomperts, R.E. Stratmann, O. Yazyev, A.J. Austin, R. Cammi, C. Pomelli, J.W. Ochterski, P.Y. Ayala, K. Morokuma, G.A. Voth, P. Salvador, J.J. Dannenberg, V.G. Zakrzewski, S. Dapprich, A.D. Daniels, M.C. Strain, O. Farkas, D.K. Malick, A.D. Rabuck, K. Raghavachari, J.B. Foresman, J.V. Ortiz, Q. Cui, A.G. Baboul, S. Clifford, J. Cioslowski, B.B. Stefanov, G. Liu, A. Liashenko, P. Piskorz, I. Komaromi, R.L. Martin, D.J. Fox, T. Keith, M.A. Al-Laham, C.Y. Peng, A. Nanayakkara, M. Challacombe, P.M.W. Gill, B. Johnson, W. Chen, M.W. Wong, C. Gonzalez, J.A. Pople, Gaussian 03, Revision C. 02, Gaussian, Inc, Wallingford, CT, 2004.
- [15] S.R. Flom, P.F. Barbara, *Chem. Phys. Lett.* 94 (1983) 488–493.
- [16] M. Wagener, J. Sadowsky, J. Gasteiger, *J. Am. Chem. Soc.* 117 (1995) 7769–7775.
- [17] Y. Yang, W.J. Zhang, X.M. Gao, *Int. J. Quantum Chem.* 106 (2006) 1199–1207.
- [18] P. Gayathri, J. Jayabharathi, N. Srinivasan, A. Thiruvalluvar, R.J. Butcher, *Acta Crystallogr.* E66 (2010) o1703.
- [19] Y. Porter, K.M. OK, N.S.P. Bhuvanesh, P.S. Halasyamani, *Chem. Mater.* 13 (2001) 1910–1915.
- [20] M. Narayana Bhat, S.M. Dharmaprasad, *J. Cryst. Growth* 236 (2002) 376–380.
- [21] D. Steiger, C. Ahlbrandt, R. Glaser, *J. Phys. Chem. B* 102 (1998) 4257–4260; J. Jayabharathi, V. Thanikachalam, K. Saravanan, N. Srinivasan, *J. Fluoresc.* (2010), doi:10.1007/s10895-010-0737-7.
- [22] M.Y. Ismet Kaya, *J. Fluoresc.*, in press; J. Jayabharathi, V. Thanikachalam, A. Saravanan, *J. Photochem. Photobiol. A* 208 (2009) 13–20.
- [23] S.G. Prabhu, P.M. Rao, S.I. Bhat, V. Upadaya, S.R. Inamdar, *J. Cryst. Growth* 233 (2001) 375–379; J. Jayabharathi, V. Thanikachalam, K. Saravanan, N. Srinivasan, M. Venkatesh Perumal, *Spectrochim. Acta A*, in press.
- [24] V. Crasta, V. Ravindrachary, R.F. Bharantri, R. Gonsalves, *J. Cryst. Growth* 267 (2004) 129–133.
- [25] P. Wang, P. Zhu, W. Wu, H. Kang, C. Ye, *Phys. Chem. Chem. Phys.* 1 (1999) 3519–3525.
- [26] Y. Yang, W.J. Zhang, X.M. Gao, *Int. J. Quant. Chem.* 106 (2006) 1199–1207.
- [27] S.F. Tayyari, S. Laleh, Z.M. Tekyeh, M.Z. Tabrizi, Y.A. Wang, H. Rahemi, *J. Mol. Struct.* 827 (2007) 176–187.
- [28] J. Marshal, *Ind. J. Phys.* 7213 (1988) 659–661.
- [29] G. Wang, F. Lian, Z. Xie, G. Su, L. Wang, X. Jing, F. Wang, *Synth. Met.* 131 (2002) 1–7.
- [30] M. Silverstein, F.X. Webster, *Spectrometric Identification of Organic Compounds*, Wiley, Asia, 2003.
- [31] R. Shanmugam, D.N. Sathyanarayana, *Spectrochim. Acta A* 40 (1984) 757–761.
- [32] J.F. Arenas, J.T. Lopez Navarrete, J.I. Marcos, J.C. Otero, *J. Chem. Soc. Faraday Trans.* 81 (1985) 405–416.
- [33] N. Sundarganesan, S. Ayyappan, H. Umamaheswari, B.D. Joshua, *Spectrochim. Acta A* 66 (2007) 17–27.
- [34] M. Ramalingam, M. Jaccob, J. Swaminathan, P. Venuvanalngam, N. Sundarganesan, *Spectrochim. Acta A* 71 (2008) 996–1002.
- [35] N.P.G. Roeges, *A Guide to the Complete Interpretation of Infrared Spectra of Organic Structures*, Wiley, New York, 1994.
- [36] M. Karaback, A. Coruh, M. Kurt, *J. Mol. Struct.* 892 (2008) 125–131.